Anisotropic Contributions in the Chromatographic Elution Behavior of Fullerenes and Fullertubes

Emmanuel Bourret,[*,†,‡] Steven Stevenson,[¶,§] and Michel Côté[*,†,‡]

†*Département de Physique, Université de Montréal, Complexe des Sciences, 1375 Avenue Thérèse-Lavoie-Roux, Montréal, QC H2V 0B3, Canada*

‡*Institut Courtois, Université de Montréal, Complexe des Sciences, 1375 Avenue Thérèse-Lavoie-Roux, Montréal, QC H2V 0B3, Canada*

¶*Department of Chemistry and Biochemistry, Purdue University Fort Wayne, Fort Wayne, Indiana 46805, United States*

§*FIRST Molecules Research Center, Purdue University Fort Wayne, Fort Wayne, Indiana 46805, United States*

E-mail: emmanuel.bourret@umontreal.ca; michel.cote@umontreal.ca

Abstract

The retention behavior of fullerenes and fullertubes on a PYE column in reversed-phase chromatography was investigated to clarify the influence of their shapes on the separation process. The impact of anisotropy was further elucidated using a pair potential interaction model, together with experimental data and ab initio calculations, to evaluate its contribution to various parameters characterizing the interaction models. The findings indicate that the shape of fullerenes plays a more significant role than anticipated in the retention mechanisms, highlighting the necessity of considering the shape of fullerenes and fullertubes to accurately predict their retention times. Furthermore, a phenomenological pair potential was devised to demonstrate the feasibility of precisely predicting the retention times of fullerenes and fullertubes through first-principles calculations, regardless of their shape. The existence of such a model paves the way for the development of a method to identify isomers of fullerenes from minute amounts of sample.

Introduction

Since the discovery of C_{60} in the mid-1980s,[1] fullerenes have been confined to molecules of less than 100 atoms. Larger fullerenes were quickly theorized,[2] but low yields, a wide variety of isomers, and the difficulty in isolating a specific isomer stunted the discovery of larger molecules.

The emergence of electric-arc synthesis,[3] which enables the production of macroscopic amounts of carbon soot containing fullerenes such as C_{60} and C_{70}, triggered a surge of interest in these novel forms of carbon. The development of a separation procedure using reversed-phase high-performance liquid chromatography (HPLC) quickly became the preferred technique to isolate higher fullerenes, leading to the discovery of C_{76}, C_{78}, C_{84}, C_{90} and C_{94} molecules.[4,5] Through the refinement of this procedure, several authors[6,7] observed, on various apolar columns, a chromatographic retention relationship characterized by a nearly

linear dependence of the logarithmic retention factor, $\ln k$, on the number of carbon atoms N for fullerenes up to C_{96}. Among these chromatographic procedures, the use of PYE columns featuring a [2-(1-pyrenyl)ethyl]silyl–silica stationary phase has been reported to offer superior baseline resolution,[7] increased loading capacity, and enhanced efficiency in separating fullerenes when used with an aromatic solvent such as toluene as the mobile phase.[8]

In an article in 1996, Fuchs et al.[9] described the main retention mechanism of fullerenes on a PYE phase as the result of van der Waals interactions between the fullerenes and the stationary phase. Mostly caused by the dispersion forces resulting from the interactions between the π-electrons of the pyrene groups and the fullerenes, their model made it possible to explain the elution behavior on a PYE phase of the fullerenes available at that time. The addition of a dipole-induced dipole interaction term further extended the model to describe the elution behavior of endohedral metallofullerenes (EMF).

More recently, the development of a method that allows the isolation of pristine and isomerically pure samples of fullertubes,[10] a hybrid between a fullerene and a nanotube where a tubular section is enclosed between two fullerene end-caps, made possible the discovery of increasingly long molecules[10–13] stimulating renewed interest in the field of fullerene science. With the increasing diversity of shapes that fullerenes can exhibit as they grow larger, the chromatographic elution model proposed by Fuchs et al. faces challenges in explaining the separation of isomers, as it only considers the influence of the number of atoms. Therefore, there is a need to reassess this model to account for the separation of isomers on the basis of their shapes.

To address this, the use of anisotropic polarizability has been proposed a few times, first by Sabirov[14] in 2014, then by Liu et al.[15,16] a few years later, as a better parameter to predict the chemical structure differences between various fullerenes, but little progress has been made in this direction. This paper addresses the latter issue.

In this study, we investigate how the anisotropy of fullerenes and fullertubes contributes to their chromatographic behavior in terms of the separation and differentiation of their

isomers. Our approach to elucidate the mechanistic aspects of fullerene retention involves examining their adsorption and chromatographic retention using fundamental interaction models. The impact of anisotropy is further clarified by assessing its role in various parameters that characterize interaction models. These theoretical considerations help us identify the essential components for predicting retention times and to determine factors that affect the design of chromatographic columns for fullerene separation. Furthermore, experimental data from different fullerenes and fullertubes will be examined and compared with theoretical predictions produced using a phenomenological model and quantities derived from density functional theory calculations. The findings are anticipated to shed light on the importance of anisotropy in determining the retention behavior of fullerenes and fullertubes.

Methods

Theory

In the realm of analytical liquid chromatography, the concentration of the injected sample is typically low. This means that the eluites, i.e. the sample components under investigation,[17] do not have to compete with each other for the limited surface area of the stationary phase, as the column is not overloaded. Consequently, each of the eluite molecules will migrate through the column, undergoing adsorption and desorption independently of each other, leading to their elution, which is discernible as Gaussian peaks on the chromatogram. This allows a practically linear relationship to be established between the concentrations of the eluites in the mobile phase and those adsorbed by the stationary phase at a constant temperature (isothermal conditions). This relationship, known as the adsorption isotherm, describes the equilibrium distribution of solutes between mobile and stationary phases on a chromatographic column in accordance with a certain retention mechanism.[18]

For fullerenes on a PYE column, the primary cause of retention is due to van der Waals interactions, mainly the dispersion forces between the fullerene eluite and a pyrene group.[8,9]

Developed by London[19] to describe the attraction between two nonpolar atoms separated by a distance r, the dispersion potential takes the form

$$U_{\text{disp}}^{6} \approx -\frac{3}{2}\frac{U_A U_B}{U_A + U_B}\frac{\overline{\alpha}^A \overline{\alpha}^B}{r^6} \tag{1}$$

where $\overline{\alpha}^A$ and $\overline{\alpha}^B$ denote the polarizabilities of atoms A and B, respectively, and U_A and U_B represent their average excitation energies, usually approximated equal to the ionization potential. This formula can be used for molecules as well, providing the dispersion interaction averaged over the relative orientations of the two molecules. In order to develop a model taking into account the anisotropy of the fullerenes passing through the stationary phase, it is essential to use a more general form of the dispersion potential where the orientation dependence is taken into account.

It is also worth mentioning that in cases where the fullerene has a permanent dipole (such as with EMF or egg-shaped isomers), an induction term is added to the attractive part of the interaction potential explaining the retention behavior.

In this section, our goal is to develop the necessary tools needed to model the interaction mechanisms governing the elution of fullerene molecules through a PYE stationary phase. To achieve this, we will first define the polarizabilities required for the force model and then use these polarizabilities to derive the formula for the anisotropic dispersion interaction. Following this, we will construct different anisotropic elution models and explore their interpretations.

Polarizability

The polarizability is the molecule's ability to acquire an induced dipole moment when subjected to an external electric field $\mathbf{E}$. In a weak field, the induced dipole moment can be expressed to first order as

$$\boldsymbol{\mu}_{\text{ind}} = \alpha \mathbf{E} \tag{2}$$

where α is the dipole polarizability tensor. In the coordinate system of the molecule, the polarizability is written as

$$\alpha = \begin{pmatrix} \alpha_{xx} & 0 & 0 \\ 0 & \alpha_{yy} & 0 \\ 0 & 0 & \alpha_{zz} \end{pmatrix} \tag{3}$$

where the eigenvalues can be seen as the semiaxes of an ellipsoid whose center coincides with the center of mass of the molecule.[14] This ellipsoid, conveniently named the polarizability ellipsoid and shown in Figure 1, replicates the shape of the molecule and illustrates the important orientation dependence when inducing an instantaneous dipole on a fullerene molecule.

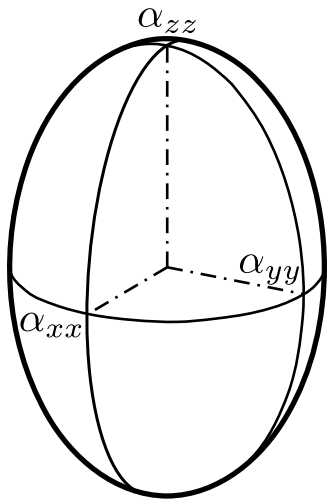

Figure 1: Polarizability ellipsoid of a molecule. The semiaxes correspond to the diagonal components of the polarizability tensor presented in eq 3.

From eq 3, two useful quantities can be defined, the isotropic polarizability $\overline{\alpha}$ and the anisotropy of polarizability $(\Delta\alpha)^2$:

$$\overline{\alpha} \equiv \frac{1}{3}(\alpha_{xx} + \alpha_{yy} + \alpha_{zz}) \tag{4}$$

$$(\Delta\alpha)^2 \equiv \frac{1}{2}\left[(\alpha_{xx} - \alpha_{yy})^2 + (\alpha_{xx} - \alpha_{zz})^2 + (\alpha_{yy} - \alpha_{zz})^2\right] \tag{5}$$

Note here that since $\Delta\alpha$ will be used for the following instead of $(\Delta\alpha)^2$ and that the units

of this quantity are the same as for a polarizability, $\Delta\alpha$ is then defined as the anisotropic polarizability. In the case of a linear fullerene molecule along the z-axis with symmetric end-caps ($\alpha_{xx} = \alpha_{yy}$), one can define the system in terms of its parallel and perpendicular components (see Section 1 of the Supporting Information). The isotropic and anisotropic polarizabilities are then written as $\overline{\alpha} = \frac{1}{3}(\alpha_{\parallel} + 2\alpha_{\perp})$ and $\Delta\alpha = \alpha_{\parallel} - \alpha_{\perp}$.

Anisotropic London Dispersion

Following the work of Stone and Tough [20], let us assume two linear fullerenes with symmetric end-caps separated by a center-to-center distance of r as shown in Figure 2.

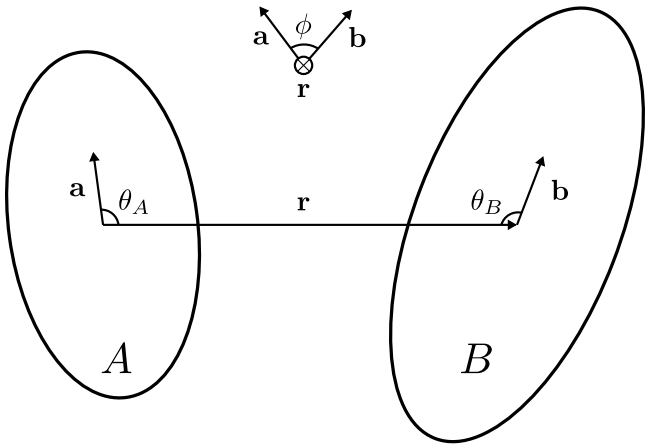

Figure 2: Schematic representation of the interaction between two anisotropic molecules. **a** and **b** are unit vectors along the axis of the molecules, and **r** is the vector through the center of molecule A to the center of molecule B. The angle between **a** and **r** is θ_A, the one between **b** and **r** is θ_B, and ϕ is the dihedral angle between two planes, one containing **a** and **r**, and one containing **b** and **r**.

The complete r^{-6} dispersion interaction then takes the form

$$\begin{aligned} U^6_{\text{disp}} = -\frac{C_6}{r^6} \Bigg\{ & 1 + \gamma_{202} \left(\frac{3}{2}\cos^2\theta_A - \frac{1}{2} \right) \\ & + \gamma_{022} \left(\frac{3}{2}\cos^2\theta_B - \frac{1}{2} \right) \\ & + \gamma_{22} \cdot \frac{1}{2} \left[\left(2\cos\theta_A \cos\theta_B - \sin\theta_A \sin\theta_B \cos\phi \right)^2 \right. \\ & \left. - \cos^2\theta_A - \cos^2\theta_B \right] \Bigg\} \end{aligned} \tag{6}$$

where the angles θ_A, θ_B and ϕ are defined as in Figure 2, and the isotropic and anisotropic dispersion coefficients are (see Section 1 of the Supporting Information)

$$\begin{aligned} C_6 &= \frac{3}{2}\frac{U_A U_B}{U_A + U_B}\overline{\alpha}^A\overline{\alpha}^B \\ \gamma_{202}C_6 &= \frac{1}{2}\frac{U_A U_B}{U_A + U_B}\Delta\alpha^A\overline{\alpha}^B \\ \gamma_{022}C_6 &= \frac{1}{2}\frac{U_A U_B}{U_A + U_B}\overline{\alpha}^A\Delta\alpha^B \\ \gamma_{22}C_6 &= \frac{1}{2}\frac{U_A U_B}{U_A + U_B}\Delta\alpha^A\Delta\alpha^B \end{aligned} \tag{7}$$

If one takes eq 6 and averages the angles over all the possible orientations, only the first term on the right-hand side remains nonzero. Consequently, only the isotropic term contributes to the dispersion interaction, and thus, we retrieve the classical formula for the London dispersion, as presented in eq 1.

Anisotropic Elution Models

In modern HPLC systems, the rapid kinetics make it possible to assume that the mobile and stationary phases are always in equilibrium.[18] The elution is then governed by the ratio between the concentrations of eluite in the mobile (C_m) and stationary (C_s) phases. With the use of standard chemical equilibrium principles, this equilibrium constant, denoted $K = C_s/C_m$, can be related to the difference in Gibbs energies associated with the transfer of eluite between the mobile and stationary phases for a reaction performed at specific pressure and temperature by

$$\Delta G^\circ = -RT\log K \tag{8}$$

where R is the gas constant and T is the absolute temperature at which the measurement is carried out. In the present case, ΔG° is approximated by the difference in energy between the fullerenes adsorbed on the stationary phase and those that are free-flowing in the bulk

mobile phase. The chromatographic retention factor, k, is also related to K by

$$k = KF \tag{9}$$

where F is the phase ratio of the column, i.e., the volume of the stationary phase divided by the volume of the mobile phase. If we substitute K with eq 9 and separate the logarithm, eq 8 becomes

$$\log k = -\frac{\Delta G^\circ}{RT} + \log F \tag{10}$$

As $F = (1 - \epsilon_\mathrm{T})/\epsilon_\mathrm{T}$, where the total porosity, denoted by ϵ_T, is a constant characterizing the packing material of the column, this equation can be written as

$$\log k = -\frac{\Delta G^\circ}{RT} + \text{constant} \tag{11}$$

In a chromatographic elution process of fullerenes on a PYE column, as the equilibrium between mobile and stationary phases is modeled by adsorption-desorption processes, the interaction potential between the phases is the London dispersion. To account for the average behavior across the column while preserving some dependence on the relative orientations of the molecules, three underlying assumptions are needed.

- Having a proportional value to r^{-6}, the dispersion potential quickly vanishes as r increases. Therefore, only the interaction between a fullerene and the nearest pyrene will be considered.

- Since the system is always assumed to be in thermodynamic equilibrium due to its rapid kinetics, ΔG° is minimal for a specific temperature and pressure. Thus, the molecules will realign in such a way that their interaction potential will be minimal, i.e. maximal attraction.

- As the kinetics are very fast, the realignment of the molecules is instantaneous on the

time scale of the molecular elution.

For the rest of this work, the molecule A is chosen to be a pyrene group of the stationary phase and the molecule B a fullerene eluite. As stated above, the transition from the orientation-dependent form of the dispersion shown in eq 6 to the isotropic expression in eq 1 is achieved by averaging the dispersion potential over the relative orientations of the molecules, specifically the angles θ_A, θ_B, and ϕ, effectively treating the molecules as polarizable spheres with polarizability $\overline{\alpha}$.

Drawing from eqs 6 and 11, there are multiple approaches to construct an elution model considering the shape of the interacting molecules in their retention mechanism. Each of them represents a different view of the microscopic activities occurring within a nonpolar column during a chromatographic elution. In the following, we will construct various anisotropic elution models and review their characteristic features.

In their groundbreaking study, Fuchs et al.[9] introduced an isotropic retention model in which it is assumed that all contacts between molecules A and B occur in random orientations as molecule B is eluted through the column. This approach simplifies the model by averaging out the angular dependencies in eq 6, resulting in eq 1. We will refer to this model as the *isotropic model*.

A first approach to incorporate an anisotropic component to the retention mechanism would be to imagine that the fullertube can reorient itself during each contact but that each contact is done with a randomly oriented pyrene molecule. This can be achieved by averaging over the angles θ_A and ϕ to leave only the dependency in θ_B. Doing so, the pyrene orientation-averaged dispersion energy can be written as

$$U^6_{\text{disp}} \approx -\frac{C_6}{r^6}\left\{1 + \gamma_{022}\left(\frac{3}{2}\cos^2\theta_B - \frac{1}{2}\right)\right\} \tag{12}$$

As previously stated, one can recognize the first term on the right-hand side of eq 12 as the dispersion potential for a pair of spherical molecules. Similarly, the anisotropic components

of the dispersion interaction between molecules A and B can also be expressed in terms of their ionization energy and static polarizabilities. Consequently, eq 12 transforms into

$$U^6_{\text{disp}} \approx -\frac{3}{2}\frac{U_A U_B}{U_A + U_B}\frac{\overline{\alpha}^A}{r^6}\left[\overline{\alpha}^B + \left(\frac{1}{2}\cos^2\theta_B - \frac{1}{6}\right)\Delta\alpha^B\right] \tag{13}$$

Because of the negative sign in front of eq 13, we want the term within the square brackets to be as large as possible. For an arbitrary distance r, this is achieved when the value of $\theta_B = 0$ or π, which corresponds to minimizing the potential energy. However, since U^6_{disp} is highly dependent on r, choosing a smaller value of r upon adsorption will consistently result in minimizing the potential energy compared to choosing a larger value for the expression within square brackets but at a greater distance. Given that r is minimized when $\theta_B = \pi/2$, it becomes evident that this angle is the optimal choice. It then follows that

$$U^6_{\text{disp}} \approx -\frac{3}{2}\frac{U_A U_B}{U_A + U_B}\frac{\overline{\alpha}^A}{r^6}\left[\overline{\alpha}^B - \frac{1}{6}\Delta\alpha^B\right] \tag{14}$$

As the term in square brackets has the units of a polarizability and only implies the eluite, let us define a new term, the effective polarizability of molecule B

$$\alpha^B_{\text{eff}} = \overline{\alpha}^B - \frac{1}{6}\Delta\alpha^B \tag{15}$$

where both the contributions of the isotropic and anisotropic polarizabilities of molecule B are taken into account. Eq 14 then becomes

$$U^6_{\text{disp}} \approx -\frac{3}{2}\frac{U_A U_B}{U_A + U_B}\frac{\overline{\alpha}^A \alpha^B_{\text{eff}}}{r^6} \tag{16}$$

A second strategy to account for anisotropy is to maintain all of the two molecules' orientation dependencies. Given the fast kinetics and that the system is at all times in equilibrium, eq 6 can thus be simplified by fixing all the angles to the values minimizing

U^6_{disp}. As with the previous approach, the important dependency of the potential in r^{-6} leads to its minimization when θ_A and θ_B are equal to $\pi/2$. Meanwhile, the angle ϕ, which has an effect on the surface of interaction between the two molecules, will minimize the potential when equal to 0. The attraction is therefore maximal when the principal axes of the two molecules are parallel. The potential can thus be expressed as

$$U^6_{\text{disp}} \approx -\frac{3}{2}\frac{U_A U_B}{U_A + U_B}\frac{1}{r^6}\alpha^{AB} \tag{17}$$

where

$$\alpha^{AB} = \overline{\alpha}^A\overline{\alpha}^B - \frac{1}{6}\left(\overline{\alpha}^A\Delta\alpha^B + \Delta\alpha^A\overline{\alpha}^B - \Delta\alpha^A\Delta\alpha^B\right) \tag{18}$$

can be understood as the polarizability coupling terms.

Using the two expressions of U^6_{disp} that we developed in eqs 16 and 17, we are now in a position to introduce two novel chromatographic relationships:

Effective model:

$$\log k = \left(\frac{ba\overline{\alpha}^A}{T}\right)\alpha^B_{\text{eff}} + c \tag{19}$$

Anisotropic model:

$$\log k = \left(\frac{ba}{T}\right)\alpha^{AB} + c \tag{20}$$

where

$$a = \frac{3}{2}\frac{U_A U_B}{U_A + U_B} \tag{21}$$

with the ionization energies U_A and U_B for the stationary phase and eluite, respectively, b is the dependency in the r given by

$$b = \frac{1}{Rr^6} \tag{22}$$

where R is the gas constant, and c is a constant of the model.

Comments on the Interpretation of the Various Models

At first glance, the three models under consideration are fairly similar to one another if we exclude how they handle the polarizability terms. A second feature that sets them apart is how we define the distance r.

Generally speaking, the center-to-center distance r can be expressed as the sum of the molecular radius of a pyrene group ρ_A, the molecular radius of the eluite ρ_B, and the distance between the surfaces of the two molecules d_{AB}:

$$r = \rho_A + \rho_B + d_{AB} \tag{23}$$

It is assumed that the carbon atoms are the primary contributors to the interaction between a fullerene and a pyrene group, and thus the value of d_{AB} should be at least 3 Å, the commonly expected minimum distance between a pair of carbon molecules in vacuum interacting through van der Waals forces. Additionally, the solvent may also contribute to the distance d_{AB}.[21]

Furthermore, the distance between the center of mass of a molecule and its surface along $\mathbf{r}$ (see Figure 2), denoted as ρ_A and ρ_B, will depend on the degree of anisotropy and the relative orientations of the molecules. For instance, when considering an eluite at adsorption in the *effective model*, ρ_B will be equal to the minimum molecular radius of the molecule B. On the other hand, the angular dependencies of the pyrene group have been averaged, so the molecule A is seen as a sphere of radius ρ_A with an isotropic polarizability of $\overline{\alpha}^A$.

As can be challenging to ascertain the values of ρ_A and ρ_B following the isotropic approximation, it would be difficult to justify an exact treatment of the *isotropic model*. However, in the *effective model*, since only ρ_A is isotropic and, above all, constant, it can be included in the value of d_{AB}. In the case of the *anisotropic model*, it can be addressed exactly as ρ_A and ρ_B are exact quantities.

Given the significance of the dependence in r^{-6} at adsorption distance, it appears from

these observations that in the case of two molecules having a similar polarizability term, a variation in ρ_B could greatly alter their relative chromatographic retention.

Another point worth dwelling on is the physical meaning of the different terms included in the definitions of α^{AB}. Expressed in terms of B, eq 18 can be rewritten as

$$\alpha^{AB} = \left(\overline{\alpha}^A - \frac{1}{6}\Delta\alpha^A\right)\overline{\alpha}^B - \frac{1}{6}\left(\overline{\alpha}^A - \Delta\alpha^A\right)\Delta\alpha^B \tag{24}$$

This equation can be used to evaluate how changes in the functional group shape affect the column's ability to separate eluites with the same isotropic polarizability. The first term in eq 24, which is always positive, indicates the contribution of the isotropic polarizability of the eluite to the retention. The second term represents the influence of the anisotropic polarizability. Depending on the relative values of $\overline{\alpha}^A$ and $\Delta\alpha^A$, the coefficient $\frac{1}{6}(\overline{\alpha}^A - \Delta\alpha^A)$ will have different effects. If $\overline{\alpha}^A > \Delta\alpha^A$, the second term in eq 24 is negative, and the anisotropy increases the separation of the different eluites. On the other hand, if $\overline{\alpha}^A = \Delta\alpha^A$, the column will be unable to separate the different eluites since the term in $\Delta\alpha^B$ will be zero. This occurs, in the case of a monoaxial molecule, when $\alpha_{\parallel} = \frac{5}{2}\alpha_{\perp}$. Lastly, if $\overline{\alpha}^A < \Delta\alpha^A$, the second coefficient will become positive and will enable the separation of the different molecules that share the same values of $\overline{\alpha}^A$.

A similar analysis can be done by expressing eq 18 in terms of A. The resulting equation will be the same as eq 24, but with A and B interchanged. From this expression, we will simply note that in the case of eluites for which the value of $\overline{\alpha}^B$ is equal to the value of $\Delta\alpha^B$, only the isotropic component of the polarizability of the functional group will affect the separation of the eluites, as when using the *effective model* presented in eq 19.

Finally, in situations where the functional group is completely isotropic, so that $\Delta\alpha^A = 0$, the *anisotropic model* is reduced to the *effective model* while maximizing the separation of eluites in the regime where $\overline{\alpha}^A > \Delta\alpha^A$.

Computational Details

To evaluate certain properties integral to the various models, we will rely on experimental observations and computed values; for example, molecular properties such as polarizabilities can be readily determined using density functional theory (DFT). All calculations were performed using the ORCA 5.0.2 software package.[22,23] All DFT calculations were carried out using the hybrid B3LYP exchange-correlation functional,[24,25] which was chosen due to its accuracy for organic systems.[26]

Geometry Optimizations

The Karlsruhe split-valence polarized basis set, def2-SVP,[27] was used to optimize all geometries. To confirm that def2-SVP is sufficient, we performed a convergence study (see Table S1) and compared the values of the orbital energies. Using this basis set, we were able to converge the orbital energies within 0.1 eV, which asserts def2-SVP completeness. The convergences for both the self-consistent field (SCF) calculation and geometry optimization were performed with an energy change threshold between two cycles of 10^{-8} hartree and 10^{-6} hartree, respectively. A fine DFT grid (DefGrid3) was used. To speed up the calculations of the Coulomb integrals, the RIJCOSX[28] approximation was used with the def2/J auxiliary basis set.[29] All geometries were optimized under vacuum conditions.

Calculation of Ionization Energies

The vertical ionization energy (IE) of a fullerene is defined as the difference of the total electronic energy between its $C_n{}^+$ and C_n form (in eV) such as

$$\mathrm{IE} = E\left(C_n{}^+\right) - E\left(C_n\right) \tag{25}$$

It was computed at the B3LYP/def2-SVP level without further thermodynamic corrections. As with orbital energies, this level of theory allows the values to converge to an unsigned

error of less than 0.1 eV (see Table S1).

Polarizabilities

All polarizability calculations were done analytically using the coupled perturbed self-consistent field (CP-SCF) method[30] in conjunction with the Rappoport property-optimized diffuse def2-SVPD basis set.[31] This set was chosen for its rapid and monotonous convergence of the isotropic polarizability of fullerenes. Compared to def2-QZVPPD, the error of the def2-SVPD basis set is below 1% (see Table S2). The CP-SCF convergence threshold over the norm of the residual vector in the solution of the CP-SCF equations was set to 10^{-4}.

Experimental Methods

The values of k were obtained experimentally by using the retention factor definition, $k = (t_\mathrm{R} - t_0)/t_\mathrm{R}$, where t_R is the retention time and t_0 is the dead time. The values of t_R were determined as the mean of a Gaussian distribution fitted to the chromatograms of the individual molecules, and their uncertainties were set at one standard deviation.

Fullerenes: Isolation of $\mathbf{C_{60}}$-I_h, $\mathbf{C_{70}}$-D_{5h}, $\mathbf{C_{76}}$-D_2, $\mathbf{C_{78}}$-C_{2v}**(2)**, $\mathbf{C_{84}}$-D_2**(22)**, and $\mathbf{C_{90}}$-C_1**(32)**

Purification of spheroidal C_{60}-I_h, C_{70}-D_{5h}, C_{76}-D_2, C_{78}-$C_{2v}(2)$, and C_{84}-$D_2(22)$ fullerenes was performed on soot extract obtained from an electric-arc synthesis (SES research, Texas, USA). To prepare a stock solution of these empty-cage fullerenes, 100 mg of soot extract was dissolved in 50 mL of *o*-xylene (2 mg mL^{-1}) and soaked overnight while stirring. After PTFE filtration to remove particulates, samples of the stock solution were injected into a 10 mm I.D. × 250 mm PYE column for HPLC separation and purification. For higher purity samples (99+%), multiple HPLC passes were performed. For quality control, a final HPLC pass and corresponding mass spectra were obtained for each fullerene isolated (see Figures S3 to S14). Isomeric purity of these fullerenes was ascertained by matching their UV-vis features with

published spectra. The isolation of spheroidal C_{90}-$C_1(32)$ was different and was successfully accomplished by injection of trace quantities of C_{90}-$C_1(32)$ which had survived the chemical reaction of soot extract with aminopropanol. See below experimental section for fullertube isolation for further details of reaction conditions.

Fullertubes: Isolation of C_{90}-D_{5h}, C_{96}-D_{3d}, C_{100}-D_{5d}, C_{114}-D_{3h}, C_{120}-D_{5d}, and C_{130}-D_{5h}

To remove the abundance of higher molecular weight empty-cage fullerene contaminants C_{76}-C_{200}, we developed a chemical purification and precleanup step for the purification of fullertubes C_{90}-D_{5h}, C_{96}-D_{3d}, C_{100}-D_{5d}, C_{114}-D_{3h}, C_{120}-D_{5d}, and C_{130}-D_{5h}. As previously described,[10,12,13] aminopropanol has demonstrated an ability to separate tubular carbon molecules (fullertubes) versus spheroidal molecular carbon (fullerenes).

For this work, we dissolved 2000 mg of carbon soot extract prepared from the flame synthesis method (Frontier Carbon, Mitsubishi, Japan) in 1200 mL of toluene. A mass spectrum of this soot extract is shown in Figure 3a. This solution (1.67 mg mL^{-1}) was allowed to soak and stir for 24 h. We added 30 mL of aminopropanol to a now vigorously stirred solution. After 90 min, the stirring was stopped. The reaction mixture was allowed to settle for 3 h and subsequently poured into a 2 L separatory funnel for 8 washes with water and 0.1 M HCl. The bottom layer (organic) contains unreacted species (i.e., family of fullertubes with residual C_{60} and C_{70} not fully removed). The mass spectrum of species (predominantly fullertubes) which survived the harsh chemical reaction with aminopropanol is shown in Figure3b.

Results and Discussion

The electronic properties of three mathematically predicted[32–34] series of fullertubes with C_{60} end-caps, namely the C_{60+10n}, C_{60+12n} and C_{60+18n} series (n is the number of carbon

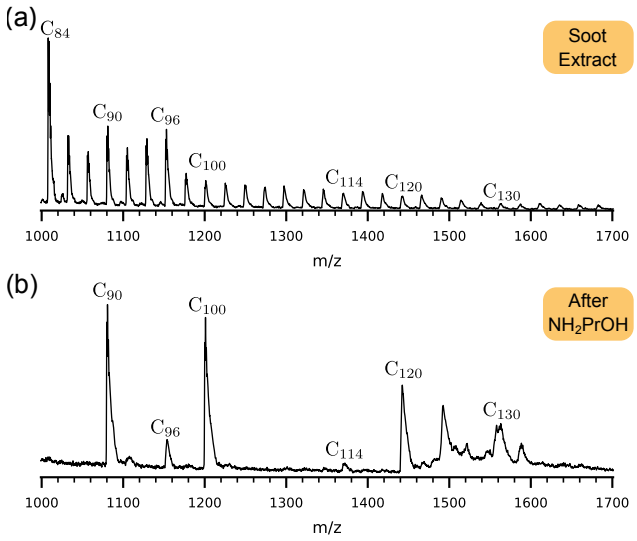

Figure 3: Laser desorption ionization mass spectra of (a) flame produced soot extract versus (b) fullertubes surviving a 90 min reaction with aminopropanol and used in HPLC purification.

belts) were examined for molecules up to 320 atoms. These tubular carbon allotropes were chosen based on the recent discovery and isolation of increasingly long members of these series.[10–13] The tubular sections specific to these series of fullertubes are related to $[5,5]$, $[9,0]$, and $[8,2]$ carbon nanotubes, respectively. Additionally, the electronic properties of six spherical fullerenes with I_h symmetry ranging from 20 to 320 atoms were evaluated for comparison. A more comprehensive list of these molecules and their properties can be found in Table S3.

To accurately assess energy trends among different molecular series, appropriate categorization is crucial. This is particularly relevant for the C_{60+10n} series of fullertubes, which, as per Harigaya[35], should be segmented into three subseries (C_{60+30n}, $C_{60+30n+10}$, $C_{60+30n+20}$) to align with the different dimerization patterns of the tubular section of these fullertubes. This hypothesis is verified in Figure 4, which shows the calculated HOMO-LUMO gaps for I_h fullerenes and the three series of fullertubes plotted against N^{-1}, where N denotes the number of carbon atoms in the molecule. Dividing the C_{60+10n} series into three distinct subseries clearly shows the different energy trends, which tend to become linear as N in-

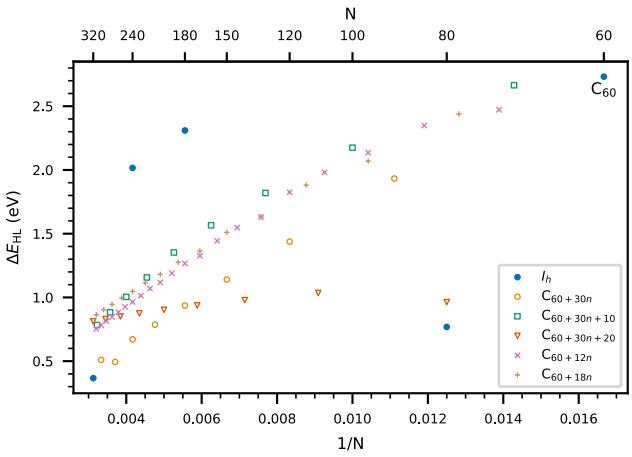

Figure 4: Calculated HOMO-LUMO gap (ΔE_{HL}) for I_h fullerenes (blue) and three series of fullertubes with C_{60} end-caps (orange, green, red, pink, tan) vs N, the number of carbon atoms. The C_{60+10n} series is divided into three distinct subseries: C_{60+30n}, $C_{60+30n+10}$, and $C_{60+30n+20}$, each corresponding to different dimerization patterns of the tubular section, as suggested by Harigaya[35]. The value calculated for C_{20}-I_h is 1.910 eV.

creases. This observation contrasts with earlier interpretations of oscillating energy trends in the C_{60+10n} series, as reported by several authors.[36,37] Similarly, the C_{60+12n} and C_{60+18n} fullertube series exhibit a linear trend as N grows. In contrast, the I_h fullerenes display more variability than the fullertube series, yet they stay within a narrow range of energy values which appear to diminish with increasing N, suggesting a general trend of decreasing gap values as the number of carbon atoms increases.

To compare the various retention models, we used the retention data listed in Table 1 that were obtained by following the experimental and computational methods described above. ρ_B is the molecular radius of the eluite in the orientation that minimizes the center-to-center distance r between an eluite molecule and a pyrenyl group on the stationary phase at adsorption. The values were determined from DFT optimized structures and those that had a significant deviation from the value for C_{60} were highlighted. The different polarizability values were calculated from eqs 4, 5, 15, and 18 with the data presented in Table S4.

Table 1: Summary of the Molecular Properties Associated with the Calculation of ΔG° for the Eluites Examined in the Present Investigation[a]

	Exptl	DFT Calculated					
Eluite	t_R [min]	ρ_B [Å]	IE [eV]	$\overline{\alpha}$ [Å^3]	$\Delta\alpha$ [Å^3]	α_{eff} [Å^3]	α^{AB} [Å^6]
				Eluites			
C_{60}-I_h	6.20 ± 0.21	3.55	7.526	81.56	0.00	81.55	2047.5
C_{70}-D_{5h}	7.33 ± 0.21	3.57	7.389	100.91	10.13	99.22	2528.2
C_{76}-D_2	8.18 ± 0.15	3.59	6.872	110.26	18.23	107.22	2758.7
C_{78}-$C_{2v}(2)$	8.48 ± 0.17	3.71[b]	7.038	112.83	17.30	109.95	2823.7
C_{84}-$D_2(22)$	9.11 ± 0.20	4.03[b]	7.025	123.45	9.59	121.86	3094.5
C_{90}-$C_1(32)$	11.17 ± 0.29	3.78[b]	6.936	134.15	21.52	130.57	3356.8
C_{90}-D_{5h}	12.00 ± 0.31	3.50	6.664	133.12	50.49	124.71	3315.8
C_{96}-D_{3d}	13.53 ± 0.27	3.54	6.736	144.58	58.83	134.77	3599.0
C_{100}-D_{5d}	18.68 ± 0.35	3.47	6.758	155.44	74.25	143.06	3863.6
C_{114}-D_{3h}	25.88 ± 0.45	3.53	6.466	181.95	108.73	163.83	4511.4
C_{120}-D_{5d}	33.64 ± 0.63	3.46	6.195	196.55	138.17	173.52	4862.3
C_{130}-D_{5h}	47.44 ± 1.06	3.44	6.366	222.86	177.16	193.34	5502.7
				Stationary phase			
Pyrene	-	-	7.161	29.50	26.37	-	-

[a]Experimental conditions: column, PYE (10 mm I.D.×250 mm); mobile phase, *o*-xylene; temperature, 22 °C; flow-rate, 3.06 mL/min; detection, UV at 500 nm; amount injected, 1000 µL. [b]Significant difference with the value for C_{60}.

Polarizability and Molecular Shape

Figure 5 shows the relationship between the calculated polarizability tensor components and the number of carbon atoms for the fullerenes and fullertubes investigated. Unsurprisingly, I_h fullerenes have values for α_{xx}, α_{yy}, and α_{zz} that are equal, demonstrating the isotropic nature of these molecules. In the case of fullertubes, the components α_{xx} and α_{yy} perpendicular to the main axis of the molecule are equal and rise linearly in N, while the parallel component α_{zz} exhibits a quadratic dependence. This is a significant difference from the quasilinear dependency previously assumed in the literature,[6,7,9] which was explained by the linear increase of the number of π-electrons in the molecules.

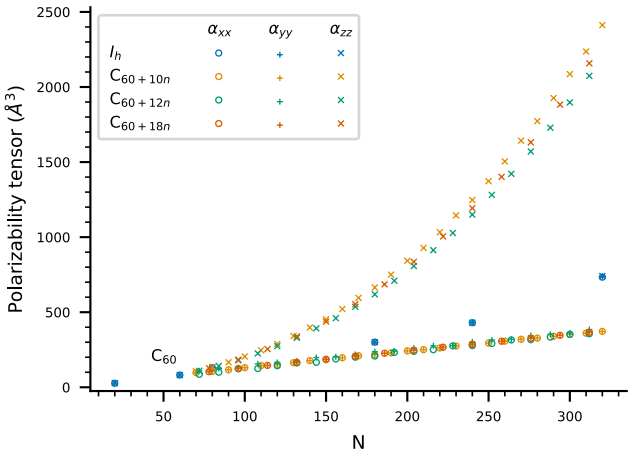

Figure 5: Calculated polarizability tensor components for I_h fullerenes (blue) and three series of fullertubes with C_{60} end-caps (orange, green, and red) vs N, the number of carbon atoms.

To illustrate how polarizabilities depend on the shape and size of the fullerene molecule, Figure 6 compares the calculated $\overline{\alpha}$ and $\Delta\alpha$, from the values presented in Figure 5, plotted as a function of the number of carbon atoms. Once again, there is an important deviation from the linearity in N of $\overline{\alpha}$. It is clear from a comparison of the I_h fullerenes with the fullertube series that the significance of the deviation is closely related to the anisotropy of the molecules. In fact, polarizability for molecules refers to the ability to transport an electronic charge q along a displacement vector $\mathbf{d}$ and induce a dipole such that $\boldsymbol{\mu}_{\text{ind}} = q \cdot \mathbf{d}$.

With the use of this definition with eqs 2 and 3, it results that

$$\alpha_{ii} = \frac{q \cdot d_i}{E_i} \tag{26}$$

It is clear from this expression that, in the presence of a constant electric field, the components of the polarizability tensor are dependent on both the charge and the distance the latter is moved on the molecule. For different isomers of the same molecule, the charge q does not change, as it is proportional to the number of π-electrons ($q \sim \mathrm{N}$).[38] However, the shape of the molecule will affect the dependency of d_i on N. If the anisotropy is minimized, as when fullerene is of spherical symmetry, the addition of carbon atoms to the molecule will increase its surface area linearly, which means that $d_i \sim \sqrt{\mathrm{N}}$ as d_i is the diameter of the molecule. If, on the other hand, the anisotropy is maximized, as with a series of tubular molecules, the addition of carbon belts will leave the perpendicular distances unchanged ($d_{x,y} \sim$ constant) but linearly increase the distance along the tubular axis, such as $d_z \sim \mathrm{N}$. Taken together, these results suggest, with eq 26, that $\alpha_{xx} = \alpha_{yy} = \alpha_{zz} \sim \mathrm{N}^{3/2}$ for spherical fullerenes, whereas $\alpha_{xx} = \alpha_{yy} \sim \mathrm{N}$ and $\alpha_{zz} \sim \mathrm{N}^2$ for fullertubes.

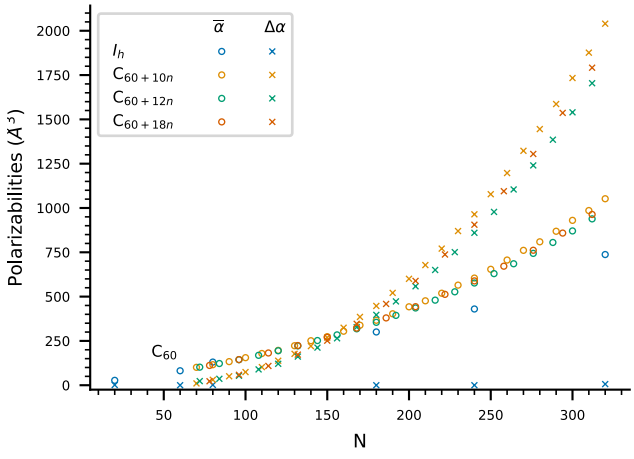

Figure 6: Calculated isotropic (∘) and anisotropic (×) polarizability for I_h fullerenes (blue) and three series of fullertubes with C_{60} end-caps (orange, green, and red) vs N, the number of carbon atoms.

This analysis is supported by the slopes obtained in Figure S1 on the logarithmic scale

graph of the calculated polatizability tensor components. For spherical fullerenes, the value obtained for the components α_{xx}, α_{yy}, and α_{zz} is 1.56. In the case of fullertubes, the slope value of 0.92 that we obtained for the components α_{xx} and α_{yy} shows that they follow a nearly linear trend, while the slope for the component α_{zz} exhibits a quadratic behavior with a value of 2.20. Since the values of $\overline{\alpha}$ and $\Delta\alpha$ in Figure 6 are derived from the polarizability tensor components presented in Figure 5 and Table S3 (see eqs 4 and 5), it can be inferred that the variation in the dependence of $\overline{\alpha}$ on N will depend on the shape of the isomer under consideration with $\overline{\alpha} \sim N^{3/2}$ for spherical fullerenes and $\overline{\alpha} \sim N^2$ for fullertubes. As these previously discussed dependencies are expected for a large value of N, the slopes were calculated for $N \geq 150$.

An interesting observation is that in the case of fullertubes with C_{60} end-caps, Figure 6 shows that the $\overline{\alpha}^B$ values correspond to those of $\Delta\alpha^B$ at around $N \approx 150$. This corresponds to the scenario in which the separation of eluites is affected only by the isotropic part of the polarizability of the functional group on the stationary phase, as elaborated following eq 24. Another noteworthy point is that both Figure 5 and Figure 6 exhibit trends in the values of the three series of fullertubes that stem from the values of C_{60} fullerene. Given that the symmetry of each I_h fullerene can be broken in three directions similar to that of C_{60} to generate series of fullertubes, it can be inferred that the polarizability values of these larger fullertube series will likely exhibit trends comparable to those of our three series of fullertubes, with the corresponding I_h fullerene as the starting point of these trends.

Ionization Energies and Molecular Radii of Fullertubes

The calculated ionization energies for I_h fullerenes and the three series of fullertubes are presented in Figure 7 against N, the number of carbon atoms. At first sight, there is a general tendency for the ionization energy to decrease as the number of atoms increases. However, when the ionization energy and the molecular radius are examined, the data points are scattered. If we focus on the different series of fullertubes, the trend is much clearer.

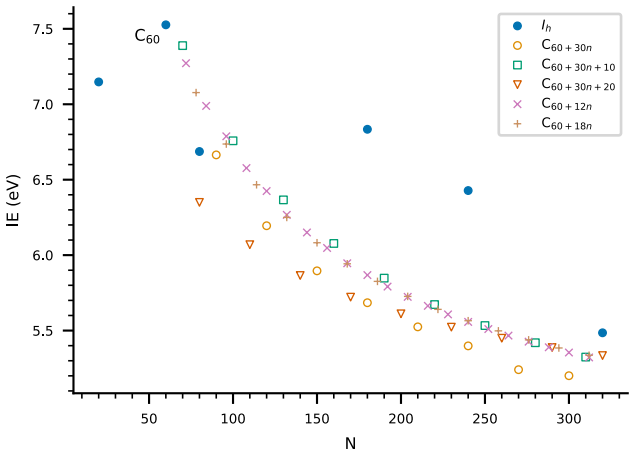

Figure 7: Calculated ionization energy (IE) for I_h fullerenes and three series of fullertubes with C_{60} end-caps vs N, the number of carbon atoms. The C_{60+10n} series was divided into three subseries (C_{60+30n}, $C_{60+30n+10}$, $C_{60+30n+20}$) according to the dimerization pattern of the tubular section following the work of Harigaya[35].

Each series decreases separately, converging toward a value that would correspond to an infinitely long fullertube, analogous to a nanotube of a given chirality. Intriguingly, the C_{60+30n} series of fullertubes appears to converge toward a marginally lower value compared to the other series. This could be indicative of a slower convergence rate for this particular series, although further investigation is required to substantiate this hypothesis. It is evident that the ionization energy strongly depends on the electronic structure of the molecule. This is demonstrated by the fact that fullertubes with similar characteristics, such as the same dimerization pattern of the tubular section or the same end-caps, share the same progression starting at the C_{60} value. We can assume that other series of fullertubes with different diameters will have similar progressions with other I_h fullerenes as their starting point; however, further research is required to verify this assumption.

Previous studies have reported a nearly linear relationship between logarithmic retention factor and polarizability.[9,10,12,13] The models, as illustrated in eqs 19 and 20 to elucidate the retention mechanism, display a linear relationship with polarizability, under the assumption that the coefficient that precedes the polarizability term, and consequently the product of the parameters b and a, stays constant. However, as demonstrated in Figure 7, the ionization

energy is heavily influenced by the fullerene's shape. As the parameter a depends on U_B, we have to question the limits of this hypothesis. It results that the product of the parameters b and a will stay constant only if their respective dependencies on r and U_B balance each other out. This is not always the case, as can be seen in Figure 8 which shows the ba product against the number of carbon atoms. The values of ba were calculated assuming a surface-to-

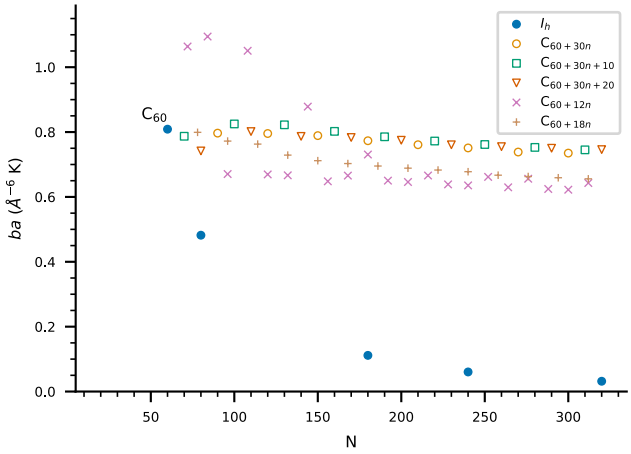

Figure 8: Dependence of the product of parameters b and a on the number of carbon atoms. The values of r used in the calculation of b were obtained by adding 3 Å to the value of ρ_B. The value calculated for C_{20}-I_h is 3.94 Å^{-6}K.

surface distance of 3 Å between the eluites and a pyrene group, to which is added the value of ρ_B when determining r for each molecule. When the tubular section of the molecules is lengthened, the values of ρ_B converge toward the radius of the related nanotubes, i.e., 3.44 Å for $[5,5]$, 3.57 Å for $[9,0]$, and 3.64 Å for $[8,2]$.

The mutual compensation of b and a is evident with the three subseries of fullertubes having a $[5,5]$ tubular section, as they have a very constant value of ba around 0.8 Å^{-6}K. Given that these fullertubes are those whose values of U_B vary the most according to Figure 7, we conclude that it is the dependence on ρ_B that dominates the values presented in Figure 8. Furthermore, the important monotonic decrease in the ba values for the I_h fullerenes as N increases also suggests a strong influence of ρ_B on this relationship, especially considering the erratic trend in their U_B values as shown in Figure 7. The significant variations observed

in Figure 8 for the smallest fullertubes of the C_{60+12n} and C_{60+18n} series are caused by the end-caps, which tend to be wider for these molecules, thus causing structural boundary conditions. This is particularly important for the first few members of the chiral C_{60+12n} fullertube series, as the squashed geometries of the end-caps give a flattened structure to the molecule when they are aligned. This results in smaller ρ_B values, thus larger ba values.

Chromatographic Retention

In Figure 9, we plot the experimental retention data obtained with empty fullerenes and fullertubes in reversed-phase chromatography employing a PYE column against DFT calculated polarizabilities for three different chromatographic models. The first model used in Figure 9a is the *isotropic model* as proposed by Fuchs et al.[9], while Figure 9b uses the *effective model* as seen in eq 19. Last, Figure 9c presents the *anisotropic model* as stated in eq 20. The parameters used to draw these plots are listed in Table 1.

It is seen for all three models that the plots are linear. For the most part, eluite molecules with greater polarizability are retained longer on the stationary phase, indicating a greater dispersion force with these molecules. However, some eluite molecules deviate from linearity. These data points correspond to fullerenes whose molecular radius is different from that of C_{60}. In order to compare the models with each other, we plotted the linear regressions obtained by using a least-squares minimization procedure. The goodness of fit can be measured by how close the value of χ^2_ν is to 1. As the importance of the molecular radius in interpreting the various models is considerable, it is essential to consider eluites with different molecular radii separately. For this reason, we repeated the fitting procedure with the subset of molecules sharing a similar value of ρ_B to that of C_{60} for comparison.

To assess which model is most suitable for describing the chromatographic behavior of fullerenes on a PYE column, it is necessary to understand the distinction between separating and differentiating eluites. Separating two eluites involves increasing the difference between their retention factor k, thus increasing the vertical distance between two molecules in Fig-

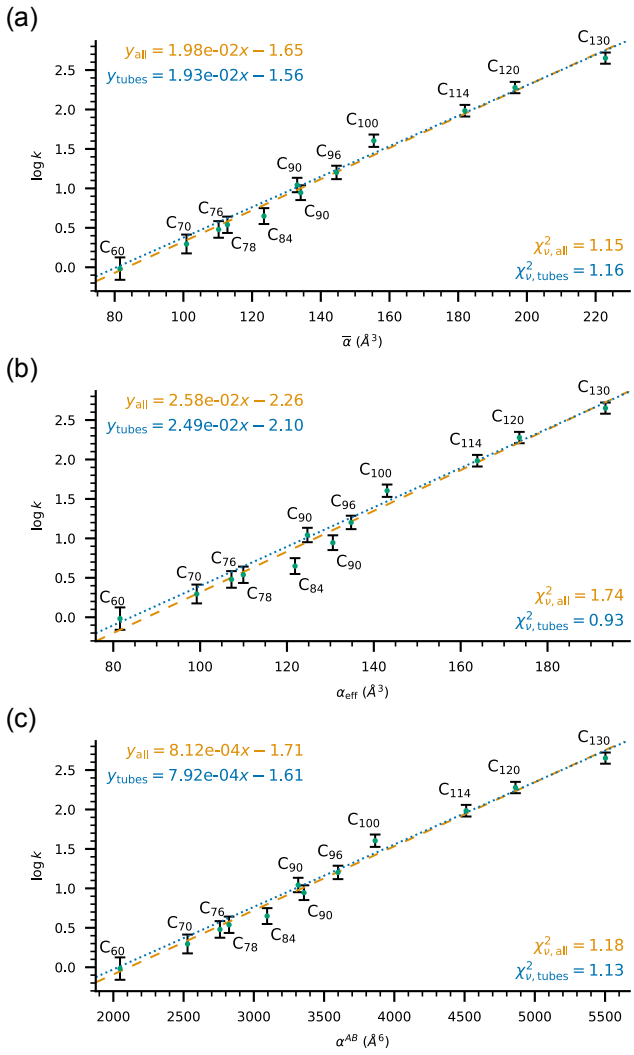

Figure 9: Logarithmic retention factors of fullerenes and fullertubes against (a) the isotropic polarizability, (b) the effective polarizability, and (c) the polarizability coupling factor. The linear regressions and the corresponding χ^2_ν statistic are shown for each model for both the whole set of molecules (dashed orange) and the subset of molecules having a radius similar to the C_{60} molecule (dotted blue). Experimental conditions as in Table 1.

ure 9. Differentiation, on the other hand, is the capacity of a model to horizontally separate two molecules whose retention times are similar on a certain reference column. Therefore, an ideal model should be able to differentiate according to a certain parameter, such as ρ_B, molecules having similar values of k while explaining the separation of eluites that share the same value of said parameter.

As seen, all linear regressions except one are a good fit with χ^2_ν values around 1. Fig-

ure 9a shows no statistically significant difference between the two data sets, indicating a low sensitivity to variation in the molecular shape of the eluites and no differentiation ability. This is not a surprise considering that the *isotropic model* treats all molecules as polarizable spheres. Figure 9b shows a higher degree of differentiation between different isomers of the same molecule. If we look for example at the case of C_{90}-$C_1(32)$, the linear slope predicts an elution at 12.56 min, i.e., after that of C_{90}-D_{5h} and in contradiction with the experimental value of 11.17 min reported in Table 1. These observations are in agreement with the theoretical considerations reported above in regard to the importance that the shape of the molecule will have on retention and explain the poor goodness of fit of the *effective model* when applied to molecules of different radii. Nevertheless, the *effective model* easily outperforms the other two models when applied only to objects of similar radius. This is because the *effective model* maximizes the contribution of the term $\Delta\alpha^B$ in eq 24 when the functional group is a pyrenyl. Figure 9c is similar to Figure 9a, except for a slightly greater differentiation between isomers of different molecular radii. This is due to the fact that the values of $\overline{\alpha}^A$ and $\Delta\alpha^A$ for pyrene are very close, resulting in a very small coefficient multiplying $\Delta\alpha^B$ in eq 24. As a result, the influence of an eluite molecule anisotropy on its retention is, according to the *anisotropic model*, virtually negligible compared to the isotropic polarizability contribution on a PYE column.

The results from Figure 9 demonstrate that the eluites whose radius differs from that of C_{60} deviate from linearity. This is due to the assumption that the slope is constant, as expressed in eqs 19 and 20, which implies that the values of r (through ρ_B) and U_B must have a relationship of mutual compensation (i.e., if U_B decreases, r must also decrease) at adsorption. However, the plot of ba against N, calculated from the values of ρ_B and ionization energy in Table 1 and shown in Figure 10, contradicts this hypothesis, thus highlighting the importance of segregation by molecular radius. This finding is supported by the improvement of the χ^2_ν in Figure 9b,c when we remove the eluites with a different ρ_B. The *effective model* is better in this regard, as it maximizes by construction the anisotropic contribution of the

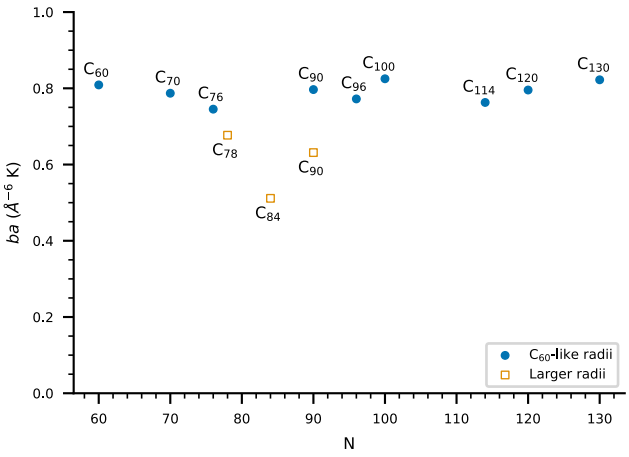

Figure 10: Dependence of the product of parameters b and a on the number of carbon atoms for the fullerenes with available experimental retention times. The calculations were done as in Figure 8.

eluites to the retention. This does not mean, however, that the model is invalid as it could be the one that best represents the average retention behavior in the column, depending on the ability of the pyrenyl groups to reorient. In contrast to the *isotropic model*, the *effective model* requires that we take into account the difference in the molecular radius of the eluites, resulting in a different curve for each series of fullerene with the same value of ρ_B. For example, if we consider only fullertubes, there would be a curve for molecules with end-caps of C_{60}, another for those with end-caps of C_{80}, and so on for all fullerenes with I_h symmetry. Our results suggest that the *effective model* is the one that best describes the average retention mechanism in a PYE column for fullertubes with C_{60} end-caps and other fullerenes with a similar value of ρ_B. However, due to the small number of fullerene or fullertube species that have the same ρ_B, but different from that of C_{60}, isolated to date, further research is needed to confirm this trend for other fullertube series.

By taking the slope values from Figure 9 and equating them to the product of eqs 21 and 22, it is possible to calculate the center-to-center distance r for each eluite. These values are presented in Table 2 for the three models and only for molecules with a similar molecular radius ρ_B. Subtracting the ρ_B values in Table 1 from these results and averaging them for each model, the average surface-to-surface distance d_{AB} is found to be 4.73 Å for the *isotropic*

model, 4.38 Å for the *effective model*, and 4.47 Å for the *anisotropic model*. These values are higher than the 3 Å usually expected between carbon molecules in vacuum. We can attribute this difference to the presence of the solvent between the molecules. Nevertheless, this does not affect the analysis of Figures 8 and 10 as all points are affected in the same way by a change of the value of d_{AB} and remain segregated by molecular radius.

Table 2: Mean Center-to-Center Distance between the Eluites and the Pyrenyl Group Calculated by Equaling the Slopes Obtained in Figure 9 to the Product of Eqs 21 and 22

Eluite	r_{iso} [Å]	r_{eff} [Å]	r_{ani} [Å]
C_{60}-I_h	8.32	7.97	8.06
C_{70}-D_{5h}	8.30	7.96	8.04
C_{76}-D_2	8.25	7.91	7.99
C_{90}-D_{5h}	8.23	7.89	7.97
C_{96}-D_{3d}	8.24	7.90	7.98
C_{100}-D_{5d}	8.24	7.90	7.98
C_{114}-D_{3h}	8.21	7.87	7.95
C_{120}-D_{5d}	8.18	7.84	7.92
C_{130}-D_{5h}	8.20	7.86	7.94

Based on these results, we can attempt to recreate the graphs shown in Figure 9 by using the calculated values of $\log k$ instead of relying on the experimental value. An example of such a graph for the *effective model* can be seen in Figure 11. The values of $\log k$ were obtained using eq 19 with the data calculated by DFT presented in Table 1. The constant was set to $\log F$, as in eq 10, where F represents the phase ratio and was experimentally determined to be 1.052.

If we now compare Figure 9b with Figure 11, we see that the general appearance of the two graphs is, at first glance, very similar. The statement holds, specifically for the series of molecules that have a radius similar to that of C_{60} (represented by blue •). This suggests that the minor deviations from linearity can be largely explained by the product of the terms b and a, which included the contribution of the molecular radius and the ionization

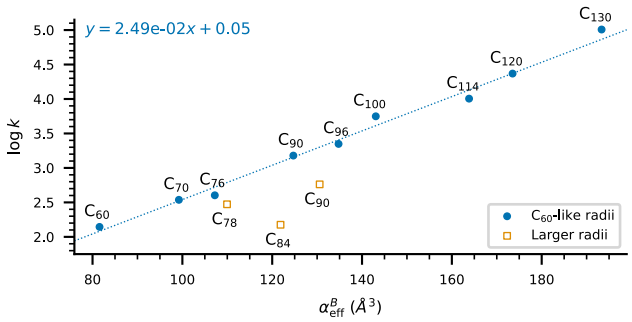

Figure 11: Calculated logarithmic retention factors of fullerenes and fullertubes against the effective polarizability. The values of $\log k$ were derived from eq 19 with the value of the constant equal to $\log F$. The linear regression is shown for the molecules having a radius similar to the C_{60} molecule (blue •). Experimental conditions as in Table 1. The phase ratio F was experimentally determined to be 1.052.

energy, respectively. However, Figure 11 shows a larger gap between the two sets of points compared to Figure 9b. This difference is expected since the value of d_{AB} used in Figure 11 was obtained without considering these fullerene molecules with a larger radius (depicted as orange □). Upon closer examination of these figures, it is evident that the values of $\log k$ are significantly higher in Figure 11 compared to Figure 9b. This observation is supported by the linear regression equations presented in both figures, which have the same slope but different y-intercepts. Hence, it can be concluded that eq 10 alone is insufficient to describe the interactions between the eluites and the stationary phase. It is important to note that the aforementioned analysis only considers the attractive interactions in vacuum between the eluites and the stationary phase. In reality, the chromatographic adsorption process occurs in a medium that is densely occupied by solvent molecules and at distances where repulsive interactions cannot be ignored. Therefore, based on Figure 11, it is evident that the models lack two important factors to accurately reproduce the experimental results: a more precise definition of the distance r, which may vary slightly depending on the molecular radius of the eluites and the presence of solvent molecules, and the inclusion of a repulsive potential to account for the significant repulsive contributions at adsorption distances.

Prediction of t_{R}

To gain a better understanding of the interactions between fullerenes and pyrenyl groups on a PYE column, it is essential to determine the exact center-to-center distance r between these two molecules. This is of the utmost importance as r plays a significant role in the retention mechanism, and the presence of solvent between the eluite molecules and the stationary phase tends to increase the separation. Consequently, predicting retention times t_{R} becomes more challenging without prior knowledge of the chromatographic behavior of species with a similar molecular radius. The linear models presented so far only consider long-range attractive interactions. This means that repulsive interactions are not explicitly considered, but are instead accounted for in the slope and intersection terms of the models through averaging. However, it is the short-distance interactions, such as Pauli repulsion, that dominate at adsorption distance. To demonstrate the feasibility of predicting retention times for various fullerenes regardless of their shape, a phenomenological pair potential was devised. This potential incorporates short-range interactions and the influence of solvent. It was constructed by adding an anisotropic repulsive potential of Born-Mayer type, as proposed by Price and Stone[39], along with a contribution from the solvent, to the models discussed so far. The aim of this exercise is to make a proof of concept to assess whether the potential can be accurately described with a unique functional form, which would ultimately allow retention time predictions to be made from first-principles calculations.

Let us consider a pyrenyl group with a solvation shell similar to those proposed by Wang et al.[21] and an eluite B located at a surface-to-surface distance d_{AB} close to the adsorption distance (to maintain relative orientations). Because there are solvent molecules between the eluite and the stationary phase, the attractive interaction between these molecules is screened. As a result, there will be a noticeable increase in the separation between the two molecules in comparison to the adsorption distance in vacuum. Given that the solvent molecules are mobile and that the attraction between them and the eluite or pyrenyl group is weaker compared to the attraction between the eluite and the pyrenyl group, it can be

inferred that the solvation shell will act as an elastic layer. Consequently, the distance d_{AB} will change as

$$d_{AB}(B) = \frac{D}{a(B)\alpha(B)} + 3 \tag{27}$$

where d_{AB} is inversely proportional to the attraction between the eluite and the pyrenyl group, while maintaining the minimum distance of 3 Å expected between carbon molecules. The inverse relationship is determined by a positive fitted parameter D, as well as the parameters a and α derived from the expression of the attractive potential described earlier. Hence, we can express the mean center-to-center distance presented in eq 23 as

$$r_{AB}(B) = \rho_B + d_{AB}(B) \tag{28}$$

With that in mind, the model potentials used for an eluite B were of the form

$$U(r, B) = \exp\{-\delta[r - \rho(B)]\} + \kappa[r - r_0(B)]^2 + U^6_{\text{disp}}(r, B) \tag{29}$$

with $\rho(B) = \rho_0 + \rho_B$ and $r_0(B) = \rho_B + 3$. The first term on the right side of the expression represents the Born-Mayer repulsive potential. It includes the term $\rho(B)$, which can be seen as a collision diameter dependent on the radius of the absorbed eluite and a fitted parameter ρ_0. The factor δ is also included to introduce the hardness of the repulsive wall. The second term in the expression is also repulsive in nature. Its purpose is to reduce the attractive potential by emulating the presence of an elastic solvation shell between the eluite and the pyrenyl group. This reduction is inversely proportional to the strength of the attraction. The term includes $r_0(B)$, which represents the expected center-to-center distance between the fullerene eluite and the pyrenyl group upon adsorption in vacuum. The final term in the expression is the attractive potential described earlier.

To determine the optimal parameters, we used a least-squares optimization procedure to fit the experimental data in Table 1 to the models. Specifically, we substituted ΔG° in

eq 10 with $U(r_{AB}, B)$ from eq 29 for both the *effective* and *anisotropic models*. The resulting parameters are listed in Table 3. At first glance, the values of these parameters appear to be consistent with their expected significance.

Table 3: Potential Parameters

Model	α [Å^6]	δ [Å^{-1}]	ρ_0 [Å]	$\kappa/10^{-2}$ [kJ mol^{-1} Å^{-2}]	$D/10^6$ [kJ mol^{-1}Å^7]
Eff.	$\overline{\alpha}^A\alpha_{\text{eff}}^B$	5.446	4.97	7.244	5.171
Aniso.	α^{AB}	3.716	4.94	5.947	4.375

The formula to calculate retention times can be derived using the relationship $k = (t_R - t_0)/t_0$ in conjunction with eq 10. The resulting equation is presented as follows:

$$t_{\text{R}} = t_0 F \exp\left(-\frac{\Delta G^\circ}{RT}\right) + t_0 \tag{30}$$

By substituting ΔG° with $U(r, B)$ from eq 29 for $r = r_{AB}$ and using the parameters listed in Table 3, we can now attempt to calculate the retention times. It should be noted that all remaining parameters are fixed constants related to the experimental setup. Tables 4 and 5 present the calculated retention times and their statistical deviations from the experimental values for both the *effective* and *anisotropic models* (see the Supporting Information for the definitions of the applied standard statistical measures). On average, the predicted times appear to be slightly underestimated, as indicated by the negative mean error (ME) value of $-0.1\,\%$. Nonetheless, Table 5 displays, for both models, small values of mean absolute error (MAE), standard deviation (SD), and absolute maximum error (AMAX). This indicates a close agreement with the experimental measurements, suggesting that our simple pair potential models have successfully captured the essential interactions of the system. It should be noted that this level of agreement is unexpected given the simplicity of the model, which only involves four fitted parameters.

Furthermore, the resulting potentials, shown in Figure 12 for the *anisotropic model*,

Table 4: Experimental and Calculated Values of Retention times[a]

		Exptl	Calculated	
Eluite	ρ_B (Å)	t_{R} (min)	$t_{\mathrm{R}}^{\mathrm{eff}}$ (min)	$t_{\mathrm{R}}^{\mathrm{AB}}$ (min)
C_{60}-I_h	3.55	6.20 ± 0.21	6.06 (−2.3%)	6.18 (−0.3%)
C_{70}-D_{5h}	3.57	7.33 ± 0.21	7.67 (4.7%)	7.69 (5.0%)
C_{76}-D_2	3.59	8.18 ± 0.15	8.17 (−0.1%)	8.23 (0.6%)
C_{78}-$C_{2v}(2)$	3.71	8.48 ± 0.17	8.42 (−0.8%)	8.40 (−1.0%)
C_{84}-$D_2(22)$	4.03	9.11 ± 0.20	9.09 (−0.2%)	8.74 (−4.0%)
C_{90}-$C_1(32)$	3.78	11.17 ± 0.29	11.51 (3.0%)	10.86 (−2.8%)
C_{90}-D_{5h}	3.50	12.00 ± 0.31	11.30 (−5.8%)	11.71 (−2.4%)
C_{96}-D_{3d}	3.54	13.53 ± 0.27	13.99 (3.4%)	14.20 (5.0%)
C_{100}-D_{5d}	3.47	18.68 ± 0.35	18.28 (−2.1%)	18.62 (−0.3%)
C_{114}-D_{3h}	3.53	25.88 ± 0.45	26.23 (1.3%)	25.92 (0.2%)
C_{120}-D_{5d}	3.46	33.64 ± 0.63	33.16 (−1.4%)	33.84 (0.6%)
C_{130}-D_{5h}	3.44	47.44 ± 1.06	47.51 (0.1%)	47.29 (−0.3%)

[a]The calculated values are for both the *effective* and the *anisotropic models*. The retention time signed errors with the experimental values are indicated in parentheses. Experimental conditions as in Table 1.

Table 5: Statistical Deviations of the Calculated Retention Times in Table 4 from Experimental Values[a]

	Effective		Anisotropic	
Measure	(%)	(min)	(%)	(min)
ME	0.0	−0.02	0.0	0.00
MAE	2.1	0.28	1.9	0.22
SD	2.9	0.36	2.7	0.30
AMAX	5.8	0.70	5.0	0.67

[a]Negative mean errors suggest that, on average, the calculated retention times are too short.

exhibit the shape of a potential well that is typically observed for models of realistic intermolecular interactions. In general, the depth and hardness of the potential increase as the eluite becomes more polarizable. It is worth noting that the position of the potential minima tends to converge toward the distance at adsorption in vacuum, as defined in eq 23, for a d_{AB} value of 3 Å, ρ_A value of 0, and ρ_B values defined in Table 4. This observation is particularly evident when comparing the values of r at the potential minima of the two C_{90} fullerenes, for which the deviation is approximately equal to the difference in their molecular radii. The variations in the positions of the minima indicate that the screening effect of the solvent molecules on the attractive interaction between the eluite and the pyrenyl group becomes less effective as the eluite molecule becomes more polarizable. Interestingly, the average distances at adsorption obtained during the parameter optimization, represented by $\circ$ in Figure 12 for each eluite, do not correspond to the potential minima. However, they appear to converge toward the minima as the eluite's polarizability increases. The rapid flow rate of 3.06 mL/min in the chromatographic column may explain this discrepancy, as eluites with lower attractive potentials may not have, on average, enough time to be fully absorbed by the stationary phase. Finally, it is evident from Figure 12 that the potential described by eq 29 is applicable only then there is a single solvation shell separating the eluite from the pyrenyl group. This is because the term responsible for reducing the dispersion interaction causes the potential to rapidly approach infinity as r becomes excessively large. To address this issue, a possible solution could involve the use of a periodic reduction term to more accurately depict multiple solvation shells. However, for the purposes of this study, the term employed seems suitable as a first-order approximation. As a result, we conclude that it is possible to find a simple functional form that faithfully reproduces the chromatographic behavior of fullerenes and fullertubes on a PYE column, regardless of their specific geometry.

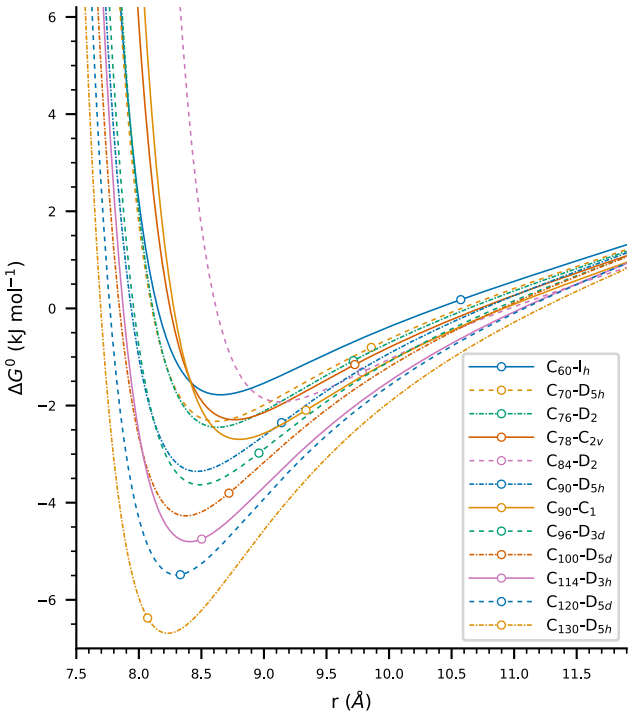

Figure 12: Potentials for the molecules listed in Table 1 predicted using eq 29 and the fitted parameter for the *anisotropic model* in Table 3. These potentials were plotted against the center-to-center distance r between the eluite and a pyrenyl group. The value of the potentials at adsorption distance r_{AB} are represented by ∘ for each eluite.

Design of the Stationary Phase

Choice of Functional Group

Putting aside the consideration on the molecular radius discussed in the previous section, the capacity of a chromatographic column to separate eluites based on their anisotropy can be affected by the shape of the functional group molecule in the context of the anisotropic retention model. Based on eq 24, we introduce a parameter to measure the contribution of the anisotropic polarizability of an eluite in comparison to its isotropic contribution, which is given by the magnitude of the ratio of the coefficient in front of $\Delta\alpha^B$ to the coefficient in front of $\overline{\alpha}^B$ as

$$\left|\frac{A_{\text{ani}}}{A_{\text{iso}}}\right| = \frac{\frac{1}{6}(\overline{\alpha}^A - \Delta\alpha^A)}{\overline{\alpha}^A - \frac{1}{6}\Delta\alpha^A} \tag{31}$$

The ratio of anisotropic to isotropic polarizability contribution, $|A_{\text{ani}}/A_{\text{iso}}|$, is a measure of

the ability of a functional group to distinguish between molecules having different shapes but the same value of isotropic polarizability. Even when this ratio is zero, i.e., when $\overline{\alpha}^A = \Delta\alpha^A$, a column can still separate two isomers of the same fullerenes since the isotropic polarizability has a certain dependence on the shape, as seen in Figure 6. However, a larger value of $|A_{\text{ani}}/A_{\text{iso}}|$ implies a greater direct contribution of $\Delta\alpha^B$ to the separation.

To further examine the relationship between the shape of the functional group and its separation ability for eluites differing by their level of anisotropy, we list in Table 6 the calculated polarizability values for different polycyclic aromatic hydrocarbons (PAH) as well as the values of $|A_{\text{ani}}/A_{\text{iso}}|$. We limited this list to planar PAHs with only hexagonal rings and whose sizes are comparable to or less than that of pyrene to allow a direct comparison with the latter. A more extensive list featuring larger PAHs and their structure can be found in Section 7 of the Supporting Information.

Table 6: Relative Contribution of the Isotropic and Anisotropic Polarizabilities to the Retention of Eluites for Different PAHs as Functional Groups

Rings	Functional Group	$\overline{\alpha}$ [Å^3]	$\Delta\alpha$ [Å^3]	$\lvert A_{\text{ani}}/A_{\text{iso}}\rvert$ [10^{-2}]
2	Naphthalene	17.64	13.72	4.26
3	Phenanthrene	25.54	22.38	2.42
3	Anthracene	26.88	27.09	0.15
4	Pyrene	29.50	26.37	2.08
4	Triphenylene	32.66	26.71	3.65
4	Benzo[c]phenanthrene	33.67	27.98	3.27
4	Chrysene	34.45	35.23	0.45
4	Benz[a]anthracene	35.50	37.16	0.95
4	Tetracene	37.84	45.45	4.19

At first glance, we see that the values of $|A_{\text{ani}}/A_{\text{iso}}|$ are usually quite small, suggesting that the term in $\overline{\alpha}^B$ is the main factor in the retention process. With the use of pyrene as a

reference, several PAHs in Table 6 could potentially give a better shape separation. With a $|A_{\text{ani}}/A_{\text{iso}}|$ ratio that is 1.75 times greater than that of pyrene, while having a slightly higher $\overline{\alpha}$ value, triphenylene seems to be the best candidate for direct comparison. To illustrate the expected effect of this substitution on separation, let us consider the two isomers of C_{90} in Table 1. With almost the same $\overline{\alpha}$ value but very different $\Delta\alpha$ values, the difference between the α^{AB} values of these two isomers is a good indicator of the effect that the shape of the functional group has on separation. With the use of the values for pyrene in Table 1, this difference is $40.97\,\text{Å}^6$. In the case of triphenylene, the values given by eq 24 have a difference of $57.78\,\text{Å}^6$, indicating a greater separation between the two isomers. In order to give the reader a better grasp of the magnitude of these results, we can also venture to predict the difference in retention time Δt_R between these two isomers if we were to elute them on various stationary phases under identical experimental conditions. This can be readily achieved by replacing the terms associated with the pyrene molecule in eq 30 with those of different PAHs listed in Table S5. As a reference, the Δt_R value predicted for the two isomers of 90 is 0.85 min on a PYE stationary phase. With triphenylene as functional group, the predicted Δt_R value is 2.52 min, suggesting a significantly larger separation of these isomers. These predictions, presented in Table S6, should be treated with caution as they are based on the assumption of a straightforward substitution of the functional group on the stationary phase, without any alterations to the packing density or any other parameters typically taken into account in column design.

Additionally, we can repeat this analysis with anthracene, which has a much smaller $|A_{\text{ani}}/A_{\text{iso}}|$ ratio than pyrene, but this time with a slightly lower $\overline{\alpha}$ value. The difference in the α^{AB} values of the two C_{90} isomers is $22.02\,\text{Å}^6$, indicating a smaller separation than with pyrene, as expected. When considering elution times, we predict a Δt_R of 0.42 min.

Naphthalene is also worth mentioning due to its large value of $|A_{\text{ani}}/A_{\text{iso}}|$, as seen in Table 6. Although it might be expected to offer the best separation, its small values of $\overline{\alpha}$ and $\Delta\alpha$ result in a α^{AB} difference of $34.74\,\text{Å}^6$ for both C_{90}. This means that the separation

by shape will be smaller than for pyrene, but the lower retention force will also lead to faster elution through the column. Our analysis is corroborated by the marginally negative value of $-0.06\,\mathrm{min}$ we predict for Δt_R, signifying a lack of separation under these conditions. This type of behavior could be beneficial for certain applications, such as the separation of larger fullertubes between 150 and 200 atoms, as their retention times on a pyrenyl phase would be impractically too long and the increasing gap between the shapes would make up for the smaller separation of naphthalene.

To better understand the relative magnitude of the polarizability terms, one can assume a functional group with the same $\overline{\alpha}$ as pyrene, but the same $|A_{\mathrm{ani}}/A_{\mathrm{iso}}|$ as another functional group. For instance, if we assume the same $|A_{\mathrm{ani}}/A_{\mathrm{iso}}|$ as for triphenylene, a possible value of $\Delta\alpha$ is $23.91\,\mathrm{\AA}^3$. This leads to a α^{AB} difference of $53.27\,\mathrm{\AA}^6$, which is very close to the value obtained with triphenylene. This suggests that small variations in the values of $\overline{\alpha}$ do not significantly affect the difference in the separation capacity between pyrene and triphenylene or between pyrene and anthracene.

Previously, we suggested that a spherical functional group would be of great interest due to its perfect isotropy. This would result in a $|A_{\mathrm{ani}}/A_{\mathrm{iso}}|$ ratio of 16.67×10^{-2}, which is the highest possible value when $\overline{\alpha}^A > \Delta\alpha^A$. However, Table S5 shows that an acene could potentially yield a higher $|A_{\mathrm{ani}}/A_{\mathrm{iso}}|$ value. As hexacene and larger acenes are known to be highly unstable,[40,41] it is unlikely that this approach is experimentally viable. Additionally, the use of a polarizability ellipsoid assumes a rigid compound, which is not a valid assumption for larger acenes. Therefore, a spherical functional group is the best choice to maximize separation by shape. This was previously demonstrated with the synthesis of a stationary phase with a chemically bonded C_{60} silica phase.[42] This column exhibited high selectivity between C_{60} and C_{70}, as well as a large retention factor.[43]

Length of the Alkyl Spacer

The alkyl spacer's length is a critical element in the design of stationary phases for fullerene separation. Despite this, the influence of the spacer is frequently overlooked in chromatographic retention models. However, the two columns most commonly used for fullerene separation, Cosmosil PYE (pyrenylethyl group) and Cosmosil Buckyprep (pyrenylpropyl group), have remarkably different retention factors, although they only differ by one carbon in the spacer.[44]

For phenyl type stationary phases, previous research has suggested that the number of carbon atoms in the spacer chain may be linked to the orientation of the phenyl ring relative to the surface of the silica.[45,46] This could be due to the fact that an even or odd number of carbons in the chain would decide the spatial orientation, either parallel or perpendicular, of the functional group relative to the surface of the silica support. However, our preliminary results indicate that for the naphthalenyl, pyrenyl, and triphenylenyl groups with ethyl or propyl spacers, both orientations are possible and the relative energy of these conformers is lower than 25.7 meV, the value of k_BT at room temperature. This suggests that a series of systematic experiments with different functional groups and spacer lengths is needed to evaluate the real effect of this parameter and that such a study would benefit from a proper conformational analysis.

Conclusion

The primary objective of this study was to explore the significance of the impact of anisotropy on the retention behavior of fullerenes and fullertubes when eluted on a PYE column in reversed-phase chromatography. The findings indicate that the dispersive interaction that occurs during the adsorption of fullerenes and fullertubes on the stationary phase is heavily influenced by the shape of the molecules. This relationship is reflected not only in the polarizability values effectively experienced by the molecules but also in the distances at which

they interact during adsorption. Therefore, it has been demonstrated that relying solely on models based on polarizability to predict the chromatigraphic retention times of fullerenes is accurate only for molecules with similar molecular radii. To predict the retention times of fullerenes regardless of their shape, it is crucial to also faithfully model the interaction distances during adsorption. The influence of solvent molecules located between the stationary phase and the eluting molecules should not be overlooked in this context. Despite these challenges, the results show that it is possible to precisely predict the retention times of fullerenes and fullertubes, regardless of their shape, by employing a streamlined pair-potential interaction model and values derived from straightforward ab initio calculations. Although the model was specifically developed to predict retention times on a PYE column, its generality should enable its application with any nonpolar fullerene separation column.

One significant use of chromatography in fullerene research is the separation of polar species, such as EMFs or egg-shaped isomers. The retention of these species is greatly influenced by their polar interactions with both the solvent and the stationary phase. To understand their retention behavior, it is essential to incorporate an attractive induction term into the model to consider these interactions. Nevertheless, further investigation is required to address this issue, as it remains uncertain whether precautions need to be taken with respect to the relative orientations of the molecules and the interaction of a polar term with solvent molecules.

The *effective model* proposed in this study demonstrates the best agreement with the retention behavior when applied to fullerenes of comparable radii. However, when compared to the anisotropic model within a framework that includes repulsion forces and considers the presence of solvent, only minor discrepancies are observed. This situation prompts inquiries into the ability of the functional groups on the stationary phase to reorient during the adsorption of an eluite molecule and the subsequent interpretation of this phenomenon. Therefore, investigating the chromatographic behavior of fullerenes and fullertubes on columns with varying spacer lengths and/or different functional groups could provide further insights into

the actual microscopic interactions occurring during an elution, potentially leading to the design of columns leveraging anisotropy for molecule separation. Moreover, it would be interesting to explore whether these frameworks can equally elucidate the chromatographic behavior of other compounds with a similar retention mechanism, such as PAHs.

It has been demonstrated that the retention times of fullerenes and fullertubes on a PYE column can be predicted by a simple functional form that incorporates ab initio parameters along with a few parameters adjusted to experimental data. Ideally, it would be preferable to predict these times solely on the basis of molecular properties derived from first principles. Since the impact of the adjusted parameters is confined to the repulsive interaction components, the primary challenge in achieving fully ab initio predictions lies in accurately determining the adsorption distances. One possible approach to address this problem may be to draw inspiration from the solvophobic theory framework proposed by Vailaya and Horváth [47,48] in the context of reversed-phase chromatography, as there are similarities in how the various terms are handled in both studies. Addressing this issue has the potential to lay the groundwork for developing a reliable model to predict retention times. Such a model could then be used as the basis for a technique to identify isomers of fullerenes and fullertubes from minute sample quantities.

Acknowledgement

This research was financially supported by the Natural Sciences and Engineering Research Council of Canada (NSERC), under the Discovery Grants program Grant RGPIN-2016-06666. This research was enabled in part by the support provided by Calcul Québec and the Digital Research Alliance of Canada. The operation of the supercomputers used for this research is funded by the Canada Foundation for Innovation (CFI), the Ministère de la Science, de l'Économie et de l'Innovation du Québec (MESI), and the Fonds de recherche du Québec – Nature et technologies (FRQ-NT). E.B. and M.C. are members of the Regroupe-

ment québécois sur les matériaux de pointe (RQMP). S.S. thanks the Chemistry Division of the National Science Foundation for Grant CHE-2247272. We thank Dr. Harry Dorn for stimulating discussions and comments.

Supporting Information Available

The Supporting Information is available free of charge at https://pubs.acs.org/doi/10.1021/acs.jpcc.4c02931.

- *xyz* coordinates of the optimized structures (ZIP)
- Mathematical analyzes, DFT convergence studies, supplementary DFT results, and structural information supporting the identification of the isolated fullerenes and fullertubes (PDF)

Notes

The authors declare no competing financial interest.

References

(1) Kroto, H. W.; Heath, J. R.; O'Brien, S. C.; Curl, R. F.; Smalley, R. E. C60: Buckminsterfullerene. *Nature* **1985**, *318*, 162–163.

(2) Fowler, P. W.; Manolopoulos, D. E. *An Atlas of Fullerenes*; International series of monographs on chemistry; Clarendon Press ; Oxford University Press: Oxford, NY, 1995.

(3) Krätschmer, W.; Lamb, L. D.; Fostiropoulos, K.; Huffman, D. R. Solid C60: a new form of carbon. *Nature* **1990**, *347*, 354–358.

(4) Diederich, F.; Ettl, R.; Rubin, Y.; Whetten, R. L.; Beck, R.; Alvare, M.; Anz, S.; Sensharma, D.; Wudl, F.; Khemani, K. C. et al. The Higher Fullerenes: Isolation and Characterization of C76, C84, C90, C94, and C70O, an Oxide of D5h-C70. *Science* **1991**, *252*, 548–551.

(5) Diederich, F.; Whetten, R. L.; Thilgen, C.; Ettl, R.; Chao, I.; Alvarez, M. M. Fullerene Isomerism: Isolation of C2v,-C78 and D3-C78. *Science* **1991**, *254*, 1768–1770.

(6) Klute, R. C.; Dorn, H. C.; McNair, H. M. HPLC Separation of Higher (C84+) Fullerenes. *Journal of Chromatographic Science* **1992**, *30*, 438–442.

(7) Anacleto, J. F.; Quilliam, M. A. Liquid chromatography/mass spectrometry investigation of the reversed-phase separation of fullerenes and their derivatives. *Anal. Chem.* **1993**, *65*, 2236–2242.

(8) Kimata, K.; Hosoya, K.; Araki, T.; Tanaka, N. [2-(1-Pyrenyl)ethyl]silyl silica packing material for liquid chromatographic separation of fullerenes. *J. Org. Chem.* **1993**, *58*, 282–283.

(9) Fuchs, D.; Rietschel, H.; Michel, R. H.; Fischer, A.; Weis, P.; Kappes, M. M. Extraction and Chromatographic Elution Behavior of Endohedral Metallofullerenes: Inferences Regarding Effective Dipole Moments. *J. Phys. Chem.* **1996**, *100*, 725–729.

(10) Koenig, R. M.; Tian, H.-R.; Seeler, T. L.; Tepper, K. R.; Franklin, H. M.; Chen, Z.-C.; Xie, S.-Y.; Stevenson, S. Fullertubes: Cylindrical Carbon with Half-Fullerene End-Caps and Tubular Graphene Belts, Their Chemical Enrichment, Crystallography of Pristine C90-D5h(1) and C100-D5d(1) Fullertubes, and Isolation of C108, C120, C132, and C156 Cages of Unknown Structures. *J. Am. Chem. Soc.* **2020**, *142*, 15614–15623.

(11) Stevenson, S.; Liu, X.; Sublett, D. M.; Koenig, R. M.; Seeler, T. L.; Tepper, K. R.; Franklin, H. M.; Wang, X.; Huang, R.; Feng, X. et al. Semiconducting and Metallic

[5,5] Fullertube Nanowires: Characterization of Pristine D5h(1)-C90 and D5d(1)-C100. *J. Am. Chem. Soc.* **2021**, *143*, 4593–4599.

(12) Liu, X.; Bourret, E.; Noble, C. A.; Cover, K.; Koenig, R. M.; Huang, R.; Franklin, H. M.; Feng, X.; Bodnar, R. J.; Zhang, F. et al. Gigantic C120 Fullertubes: Prediction and Experimental Evidence for Isomerically Purified Metallic [5,5] C120-D5d(1) and Non-metallic [10,0] C120-D5h(10766). *J. Am. Chem. Soc.* **2022**, *144*, 16287–16291.

(13) Bourret, E.; Liu, X.; Noble, C. A.; Cover, K.; Davidson, T. P.; Huang, R.; Koenig, R. M.; Reeves, K. S.; Vlassiouk, I. V.; Côté, M. et al. Colossal C130 Fullertubes: Soluble [5,5] C130-D5h(1) Pristine Molecules with 70 Nanotube Carbons and Two 30-Atom Hemifullerene End-caps. *J. Am. Chem. Soc.* **2023**, *145*, 25942–25947.

(14) Sabirov, D. S. Polarizability as a landmark property for fullerene chemistry and materials science. *RSC Adv.* **2014**, *4*, 44996–45028.

(15) Liu, X.; Zuo, T.; Dorn, H. C. Polarizability Effects Dominate the Chromatographic Retention Behavior of Spheroidal and Elipsoidal Metallofullerene Nanospheres. *J. Phys. Chem. C* **2017**, *121*, 4045–4049.

(16) Liu, X.; Dorn, H. C. DFT prediction of chromatographic retention behavior for a trimetallic nitride metallofullerene series. *Inorg. Chim. Acta* **2017**, *468*, 316–320.

(17) Borman, S. Eluent, Effluent, Eluate, and Eluite. *Anal. Chem.* **1987**, *59*, 99A–99A.

(18) Guiochon, G.; Felinger, A.; Shirazi, D. G. *Fundamentals of Preparative and Nonlinear Chromatography*; Elsevier, 2006.

(19) London, F. The general theory of molecular forces. *Trans. Faraday Soc.* **1937**, *33*, 8b–26.

(20) Stone, A. J.; Tough, R. J. A. Spherical tensor theory of long-range intermolecular forces. *Chem. Phys. Lett.* **1984**, *110*, 123–129.

(21) Wang, C. I.; Hua, C. C.; Chen, S. A. Dynamic Solvation Shell and Solubility of C60 in Organic Solvents. *J. Phys. Chem. B* **2014**, *118*, 9964–9973.

(22) Neese, F. The ORCA program system. *WIREs Computational Molecular Science* **2012**, *2*, 73–78.

(23) Neese, F. Software update: The ORCA program system—Version 5.0. *WIREs Computational Molecular Science* **2022**, *12*, e1606.

(24) Becke, A. D. Density-functional thermochemistry. III. The role of exact exchange. *J. Chem. Phys.* **1993**, *98*, 5648–5652.

(25) Lee, C.; Yang, W.; Parr, R. G. Development of the Colle-Salvetti correlation-energy formula into a functional of the electron density. *Phys. Rev. B* **1988**, *37*, 785–789.

(26) Riley, K. E.; Op't Holt, B. T.; Merz, K. M. Critical Assessment of the Performance of Density Functional Methods for Several Atomic and Molecular Properties. *J. Chem. Theory Comput.* **2007**, *3*, 407–433.

(27) Weigend, F.; Ahlrichs, R. Balanced basis sets of split valence, triple zeta valence and quadruple zeta valence quality for H to Rn: Design and assessment of accuracy. *Phys. Chem. Chem. Phys.* **2005**, *7*, 3297–3305.

(28) Helmich-Paris, B.; de Souza, B.; Neese, F.; Izsák, R. An improved chain of spheres for exchange algorithm. *J. Chem. Phys.* **2021**, *155*, 104109.

(29) Weigend, F. Accurate Coulomb-fitting basis sets for H to Rn. *Phys. Chem. Chem. Phys.* **2006**, *8*, 1057–1065.

(30) Neese, F. Prediction of molecular properties and molecular spectroscopy with density functional theory: From fundamental theory to exchange-coupling. *Coord. Chem. Rev.* **2009**, *253*, 526–563.

(31) Rappoport, D.; Furche, F. Property-optimized Gaussian basis sets for molecular response calculations. *J. Chem. Phys.* **2010**, *133*, 134105.

(32) Bodner, M.; Patera, J.; Szajewska, M. C70, C80, C90 and carbon nanotubes by breaking of the icosahedral symmetry of C60. *Acta Crystallogr., Sect. A: Found. Crystallogr.* **2013**, *69*, 583–591.

(33) Bodner, M.; Bourret, E.; Patera, J.; Szajewska, M. Icosahedral symmetry breaking: C60 to C78, C96 and to related nanotubes. *Acta Cryst A* **2014**, *70*, 650–655.

(34) Bodner, M.; Bourret, E.; Patera, J.; Szajewska, M. Icosahedral symmetry breaking: C60 to C84, C108 and to related nanotubes. *Acta Cryst A* **2015**, *71*, 297–300.

(35) Harigaya, K. From ${\mathrm{C}}_{60}$ to a fullerene tube: Systematic analysis of lattice and electronic structures by the extended Su-Schrieffer-Heeger model. *Phys. Rev. B* **1992**, *45*, 12071–12076.

(36) Cioslowski, J.; Rao, N.; Moncrieff, D. Electronic Structures and Energetics of [5,5] and [9,0] Single-Walled Carbon Nanotubes. *J. Am. Chem. Soc.* **2002**, *124*, 8485–8489.

(37) Yumura, T.; Nozaki, D.; Hirahara, K.; Bandow, S.; Iijima, S.; Yoshizawa, K. Quantum-size effects in capped and uncapped carbon nanotubes. *Annu. Rep. Prog. Chem., Sect. C: Phys. Chem.* **2006**, *102*, 71–91.

(38) Salem, L. The calculation of dispersion forces. *Mol. Phys.* **1960**, *3*, 441–452.

(39) Price, S.; Stone, A. Evaluation of anisotropic model intermolecular pair potentials using an ab initio SCF-CI surface. *Molecular Physics* **1980**, *40*, 805–822.

(40) Anthony, J. E. The Larger Acenes: Versatile Organic Semiconductors. *Angew. Chem., Int. Ed.* **2008**, *47*, 452–483.

(41) Mondal, R.; Tönshoff, C.; Khon, D.; Neckers, D. C.; Bettinger, H. F. Synthesis, Stability, and Photochemistry of Pentacene, Hexacene, and Heptacene: A Matrix Isolation Study. *J. Am. Chem. Soc.* **2009**, *131*, 14281–14289.

(42) Saito, Y.; Ohta, H.; Terasaki, H.; Katoh, Y.; Nagashima, H.; Jinno, K.; Itoh, K. Separation of polycyclic aromatic hydrocarbons with a C60 bonded silica phase in microcolumn liquid chromatography. *Journal of High Resolution Chromatography* **1995**, *18*, 569–572.

(43) Schurig, V. *Applications of Supramolecular Chemistry; Schneider, H.-J., Ed*; CRC Press: Boca Raton, FL, USA, 2012; pp 129–157.

(44) nacalai tesque: Fullerene Separation Columns. 2023; `https://www.nacalai.co.jp/global/cosmosil/column/11.html`, (accessed 2023-10-12).

(45) Kayillo, S.; Dennis, G. R.; Shalliker, R. A. An assessment of the retention behaviour of polycyclic aromatic hydrocarbons on reversed phase stationary phases: Selectivity and retention on C18 and phenyl-type surfaces. *Journal of Chromatography A* **2006**, *1126*, 283–297.

(46) Stevenson, P. G.; Mayfield, K. J.; Soliven, A.; Dennis, G. R.; Gritti, F.; Guiochon, G.; Shalliker, R. A. π-Selective stationary phases: (I) Influence of the spacer chain length of phenyl type phases on the aromatic and methylene selectivity of aromatic compounds in reversed phase high performance liquid chromatography. *Journal of Chromatography A* **2010**, *1217*, 5358–5364.

(47) Vailaya, A.; Horváth, C. Solvophobic Theory and Normalized Free Energies of Nonpolar Substances in Reversed Phase Chromatography. *J. Phys. Chem. B* **1997**, *101*, 5875–5888.

(48) Vailaya, A.; Horváth, C. Retention in reversed-phase chromatography: partition or adsorption? *Journal of Chromatography A* **1998**, *829*, 1–27.

TOC Graphic

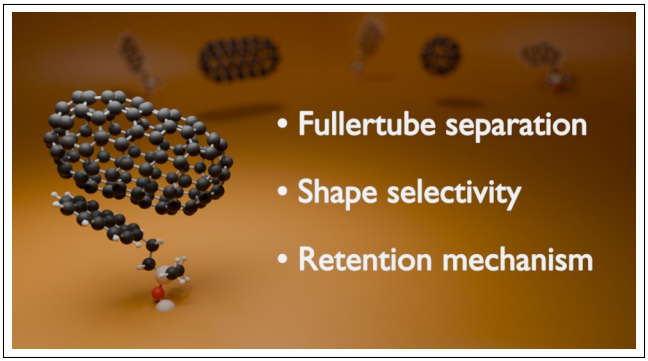
• Fullertube separation
• Shape selectivity
• Retention mechanism